HHS Public Access

Author manuscript

J Biomed Mater Res A. Author manuscript; available in PMC 2018 September 28.

Published in final edited form as:

J Biomed Mater Res A. 2018 August ; 106(8): 2213–2228. doi:10.1002/jbm.a.36428.

A collagen based cryogel bioscaffold coated with nanostructured polydopamine as a platform for mesenchymal stem cell therapy

Mehdi Razavi, **Sophia Hu**, and **Avnesh S. Thakor**

Department of Radiology, Stanford University, Palo Alto, California 94304

Abstract

Cryo-hydrogels (cryogels) are polymer hydrogels formed at sub-zero temperatures. Bioscaffolds created from cryo-gels have interconnected macropores which allow for cell migration, tissue-ingrowth, unhindered diffusion of solutes and mass transport of therapeutics. In this study, we developed collagen based cryogel bioscaffolds and coated them with polydopamine using a simple two-step technique. Cryogel bioscaffolds were synthesized by collagen crosslinking at −20°C and exhibited a macroporous interconnected architecture with 75% ± 63% porosity. Two groups of pore sizes were observed: 300 ± 50 μm and 30 ± 10 μm in diameter. The addition of a polydopamine coating to cryogel bioscaffolds was confirmed using composition analysis. This resulted in a 41% ± 6 5% decrease in water uptake, 81% ± 10% decrease in swelling rate and 12% ± 3% decrease in their degree of dissolution ($p < 0.05$), with a 48% ± 2% increase in stiffness and 57% ± 5% increase in compressive strength ($p < 0.05$). Seeding adipose tissue-derived mesenchymal stem cells (AD-MSCs) into polydopamine coated-cryogel bioscaffolds resulted in cells demonstrating a 52% ± 4% increase in viability and 33% ±3% increase in proliferation when compared to ADMSCs seeded into uncoated-cryogel bioscaffolds ($p < 0.05$). In summary, our novel polydopamine coated-cryogel bioscaffold represents an efficient and low-cost bioscaffold platform to support MSC therapies.

Keywords

cryogel; bioscaffold; polydopamine; mesenchymal stem cells; regenerative medicine

INTRODUCTION

Regenerative medicine offers the potential to significantly impact a wide spectrum of healthcare issues from diabetes to cardiovascular disease.[1] One area which has attracted significant attention is the development of novel 3D porous bioscaffolds which can accommodate different types of cellular therapy. Bioscaffolds can be created from a plethora of biomaterials which can be specifically chosen based on their (1) intrinsic properties, (2)

Correspondence to: A. S. Thakor; asthakor@stanford.edu.

CONFLICT OF INTEREST

The authors have declared that there is no conflict of interest.

ability to integrate into the host tissue, and (3) ability to create an optimal microenvironment to nourish and support cells.

Hydrogels constitute a group of polymeric materials that are capable of holding large amounts of water within their 3D network. Hydrogels have an innate structural and compositional similarity to tissue extracellular matrix (ECM), thereby making them an attractive 3D bioscaffold biomaterial for clinical translation. Furthermore, they can be developed with different chemical and physical properties based on a wide variety of chemical building blocks and synthetic techniques. This enables the properties of hydrogels to be tailored such that cellular attachment, biodegradability and biocompatibility can all be optimized to suit specific applications.[2]

Recently, cryo-hydrogels (that is, cryogels) have gained interest due to their larger interconnected macropores (that is, super-macropores) and enhanced mechanical stability compared to traditional hydrogel constructs. The macroporous structure of cryogel enables cells to interact with, and migrate into, the substrate with considerable ease. Cryogels are made at temperatures below the freezing point of a bulk solvent, which creates ice crystals during the frozen phase. Melting of these ice crystals at higher temperatures then gives rise to an interconnected macroporous cryogel network.[3,4]

Although cryogels can be made from different kinds of biopolymers such as alginate,[5] polyacrylonitrile,[6] gelatin,[7] and chitosan,[8] collagen is one of the most prevalent cryogel precursors since it is a primary component of the ECM of mammalian connective tissue. Furthermore, collagen is readily available, has a fibril architecture that is similar to natural tissues and demonstrates reduced biodegradability which therefore makes it a desirable biomaterial in regenerative medicine.[9,10] In order to improve the adhesion and proliferation of cells seeded into collagen bioscaffolds, a variety of approaches have been employed to treat their surface which includes using multi-walled carbon nano-tubes,[11] apatite,[12] and β-tricalcium phosphate.[13] However, these processes are usually limited by tedious preparation steps and rigorous reaction conditions.[14] Polydopamine coating has recently become a safe way to address these shortfalls, especially given that there is no need to use toxic chemicals.[15] Inspired by the composition of adhesive proteins from mussels, thin surface-adherent polydopamine films can be easily formed and strongly adhered onto a wide range of inorganic and organic materials, including noble metals, oxides, polymers, semiconductors, and ceramics.[16] Polydopamine coating can be applied through a simple dip-coating of objects for 0.5–2 h in an aqueous solution of dopamine which is an inexpensive material compared to the abovementioned coating materials, thereby reducing both the *coating time and procedural cost*.[14]

Hence, in the present study we aimed to improve the biocompatibility of our collagen based cryogel bioscaffold by applying a polydopamine coating using a simple, environmentally safe and effective surface functionalization technique.[17] Dopamine undergoes oxidative polymerization in alkaline conditions to form polydopamine, which has a strong adsorption onto a wide variety of substrates through its covalent bonding and strong intermolecular interactions from its repeating 3,4-dihydroxy-L-phenylala-nine-lysine (DOPA-K) motif.[16] Studies have shown that polydopamine coating also reduces substrate surface

hydrophobicity[18] and stimulates *in vitro* tissue formation.[19–21] In addition, polydopamine has been shown to reduce the *in vivo* toxicity of implanted biomaterials because of its excellent biocompatibility while also providing a surface for the conjugation of a wide variety of molecules via simple chemical reactions.[22]

The interaction between mesenchymal stem cells and biomaterials has received considerable interest in regenerative medicine.[23] Adipose tissue derived mesenchymal stem cells (AD-MSCs) have been used in our study since they have been shown to have a greater regenerative capacity when compared to conventional bone marrow (BM)-MSCs.[24] Furthermore, AD-MSCs can be isolated with high yield from adipose tissue obtained during routine liposuction/lipoplasty procedures without the use of enzymes or the need for *ex vivo* expansion.[25] AD-MSCs have been shown to secrete a large spectrum of bioactive molecules which create a unique microenvironment for the regeneration of injured tissues.[26] As AD-MSCs are also immuno-protective and can facilitate cellular survival through the release of trophic factors, several studies are investigating their ability to be co-transplanted with different organs to improve cell engraftment and survival (that is, the cotransplantation of AD-MSCs and pancreatic islets for the treatment of type 1 diabetes).[27–29] Hence, in the present study, we developed a collagen-based cryogel bioscaffold and coated it with polydopamine. We then evaluated the structural and mechanical properties of this bioscaffold in addition to determining its ability to facilitate the survival and growth of AD-MSCs.

MATERIALS AND METHODS

Bioscaffold synthesis

Collagen, sourced from bovine achilles tendon (Sigma-Aldrich), was dispersed in 5 m*M* hydrochloric acid (HCl; Fisher Scientific) and swollen overnight at 48°C at a concentration of 3% (wt/vol). The acid-swollen collagen slurry was centrifuged at 10,000 rpm for 10 min to separate the HCl from the collagen slurry. In order to create a collagen based cryogel, 5 ml of the collagen slurry was diluted in 8 ml of 5 m*M* HCl in an ice bath. To start the collagen cross-linking process, 15 m*M* N-hydroxysuccinimide (NHS; Fischer Scientific) and 30 m*M* 1-ethyl-3–(3-dimethylaminopropyl) carbodiimide hydrochloride (EDC; Fischer Scientific) were both added to the collagen slurry which was then transferred into a prefabricated mold and kept in a freezer at −20°C for 24 h. After 24 h, the cryogel was thawed at room temperature in order to create 3D macroporous cryogel bio-scaffolds [Fig. 1(a)]. All bioscaffolds were then washed three times with distilled water to ensure removal of all the chemicals before being sectioned in their wet state. A Kim-wipe was then used to wick away any residual water before leaving bioscaffolds to dry at room temperature for 24 h.

Bioscaffold coating

Polydopamine solutions are pH and light sensitive and hence need careful handling. The coating process was therefore performed at pH 8.5 in the dark.[30] Synthesized bioscaffolds were immersed in a dopamine solution (2 mg/ml in 10 m*M* Tris) to self-polymerize the dopamine before being placed on a tube rotisserie at 18 rpm for 30 min at 25°C [Fig. 1(b,c)].

Polydopamine coated-cryogel bioscaffolds were then washed three times with distilled water to remove any deposited polydopamine micro-particles and/or excess Tris.

All analyses were then performed on the same size (discs measuring 5 mm thick × 10 mm diameter) and weight (30 mg) of uncoated- and polydopamine coated-cryogel bioscaffolds in their dry state.

Bioscaffold porosity and density measurement

i. Porosity: The porosity of each bioscaffold was calculated in their dry state using the equation below (Eq. 1):

$$\text{Porosity}(\%) = \frac{\frac{W_s - W_d}{\rho_w}}{\frac{W_s - W_d}{\rho_w} + \frac{W_d}{\rho_s}} \quad (1)$$

where W_s is the weight of the saturated bioscaffold, W_d is the weight of the dried bioscaffold, ρ_w is the density of water and ρ_s is the density of the bioscaffold.

ii. Density: The volume of each bioscaffold was calculated using the height and diameter of sectioned samples. The volume to weight ratio was then used to obtain each bioscaffold density ($g.cm^{-3}$) using the equation below (Eq. 2):

$$\rho = \frac{W}{\pi \times \frac{D^2}{4} \times H} \quad (2)$$

where ρ is the density, W is the dry weight in grams, D is the diameter in cm and H is the thickness of a bioscaffold in cm. Bioscaffold porosity and density measurements were performed on three separate samples from each of the following experimental groups: (1) uncoated and (2) polydopamine coated-cryogel bioscaffolds.

Bioscaffold structural and chemical analysis

i. Scanning electron microscopy (SEM): Bioscaffolds were dehydrated using 10 min sequential immersions through a standard sequence of 50, 70, 90, and 100% ethanol solutions. A Kimwipe was then used to wick away any ethanol solution before allowing bioscaffolds to dry overnight at room temperature to prevent bioscaffolds from cracking during the SEM preparation process. Bio-scaffolds were finally coated with Au-Pd using a sputter coater and their morphology was analyzed by a SEM (XL30 Sirion, FEI). SEM was performed on three separate samples from each of the following experimental groups: (1) uncoated and (2) polydopamine coated-cryogel bioscaffolds. At five random locations within each sample, the pore size were measured.

ii. Micro-computed tomography (μ-CT): Bioscaffolds were scanned in a consecutive manner using a high-resolution μ-CT (VivaCT 40, Switzerland) to analyze their 3D architecture and porosity. μ-CT was performed on one sample from each of the following experimental groups: (1)uncoated and (2) polydopamine coated-cryogel bioscaffolds.

iii. X-ray photoelectron spectroscopy (XPS): Both qualitative and quantitative information about the presence of different elements on the surface of bioscaffolds were scanned using a VersaProbe 1 Scanning XPS Microprobe with a monochromatic Al K alpha X-ray source (ULVAC-PHI, Physical Electronics) in both survey and high-resolution modes. The survey scan was performed with the pass energy of 117.4 eV, the range of 0–1400 eV, energy step of 1 eV, time/step of 20 ms for three cycles. The high-resolution scan of C1s, N1s and O1s was performed with the pass energy of 23.5 eV, energy step of 0.1 eV and time/step of 50 ms for three cycles. All spectra were collected with the charge neutralization flood gun turned on. Data were processed using the MultiPak program XPS software package. Since, sample exposure to atmospheric conditions results in spontaneous physisorption of C, N, and O onto the bioscaf-fold surfaces, the samples were sectioned immediately before XPS analysis and the cross-sectioned surface was analyzed. XPS was performed on three separate samples from each of the following experimental groups: (1) uncoated and (2) polydopamine coated-cryogel bioscaffolds.

iv. Attenuated total reflection-fourier transform infrared (ATR-FTIR): Bioscaffolds were scanned over a frequency region of 400–4000 cm^{-1} using an ATR-FTIR (Nicolet iS50 FT/IR) spectrometer and the characteristic peaks of infrared transmission spectra recorded. ATR-FTIR was performed on 3 separate samples from each of the following experimental groups: (1) uncoated and (2) polydopamine coated-cryogel bioscaffolds.

v. Raman spectroscopy: The Raman spectra of bioscaffolds were acquired over a Raman shift region of 0–3500 cm^{-1} using a micro-Raman confocal scanning microscope (WiTec 500). Raman spectroscopy was performed on 3 separate samples from each of the following experimental groups: (1) uncoated and (2) polydopamine coated-cryogel bioscaffolds.

Bioscaffold water uptake, swelling, and biodegradability

i. Water uptake and swelling: The dry weight of each bio-scaffold was initially recorded prior to any experiment, followed by its corresponding wet weight at specific time points (0, 0.5, 1.5, 3.5, 6.5, 10.5, 15.5, 22.5, and 32.5 min) following immersion in deionized water. These time points were chosen to show the dynamic rate at which bioscaffolds can uptake deionized water. Given that there were only minimal increases in water uptake between 6 and 32.5 min, all bioscaffolds were then dried at 32.5 min at 50°C in an oven. Hydration cycles were then repeated with assessments of water uptake at the same time intervals for a total of three consecutive cycles. The percent of water uptake [W_u (%)] and swelling ratio S_R in bioscaffolds at each time point was calculated using following equations (Eqs. 3 and 4):

$$W_u(\%) = \frac{W_t - W_d}{W_{s32.5}} \times 100 \quad (3)$$

$$S_R = \frac{W_t}{W_d} \quad (4)$$

where W_t is the weight of the swollen bioscaffold at a chosen time point, W_d is the weight of the dry bioscaffold and $W_{s32:5}$ is the weight of the swollen bioscaffold at 32.5 min. Bioscaffold water uptake was measured on three separate samples from each of the following experimental groups: (1) uncoated and (2) polydopamine coated-cryogel bioscaffolds. Bioscaffold swelling was measured on three separate samples from each of the following experimental groups: (1) uncoated and (2) polydopamine coated-cryogel bioscaffolds.

ii. Biodegradability: Each bioscaffold was weighed (dry weight: W_{d1}) and then incubated in sterile phosphate buffered saline (PBS) for up to 4 weeks. At week 1, 2, and 4, all bioscaffolds were removed from the PBS, dried overnight at 508C and then re-weighed (dry weight [W_{d2}]). The degree of dissolution of bioscaffolds was calculated using the following equation (Eq. 5):

$$\text{Biodegradability}(\%) = \frac{W_{d1} - W_{d2}}{W_{d1}} \times 100 \quad (5)$$

Bioscaffold biodegradability was measured on three separate samples from each of the following experimental groups: (1) uncoated and (2) polydopamine coated-cryogel bioscaffolds.

Bioscaffold rheological and mechanical properties

i. Rheology: The flow behavior and viscoelastic properties of bioscaffolds were studied using a high-resolution and double wall ring interfacial rheology system (TA Instrument ARES-G2) with a parallel plate geometry (25 mm diameter and 1 mm gap) set at 37°C. Rheological analysis was performed in the wet state by saturating bioscaffolds with PBS. Chemically cross-linked polymers undergo a solid to liquid transition, in which both the sol- and gel-like characteristics can be observed before and after gel-point. The rheological spectra were obtained using oscillation rheology to measure three parameters of G' (storage modulus), G'' (loss modulus) and Tan δ (phase angle) as a function of ω (angular frequency), γ (oscillation strain) and ts (time per step) in the frequency range of 0.1–100 rad/s, oscillation strain range of 0.1–1000 and step time range of 0–300 s, respectively. The solid (G') and liquid (G'') behaviors of the material were measured using Eqs. 6 and 7, respectively.

$$G' = Cos\ \delta \left(\frac{\sigma_0}{\gamma} \right) \quad \text{(Eq. 6)}$$

$$G'' = Sin\ \delta \left(\frac{\sigma_0}{\gamma} \right) \quad \text{(Eq. 7)}$$

where σ_0 is the shear stress, γ is the amplitude of the strain response and δ is the phase angle (angle between the applied and measured stress response).[31] The Tan δ is the difference in waveform shift that is recorded when a force is applied and a response to the force is generated. A phase angle value closer to 0 indicates that a material is more elastic while as the phase angle value closer to 90 indicates viscous nature of a material.[32] The storage modulus (G') is directly related to the crosslink density (ν_c) according to the Eq. (8):[21]

$$G' = \upsilon_c R T \quad (8)$$

Where T is the temperature and R is the gas constant. Bioscaffold rheological properties were measured on three separate samples from each of the following experimental groups: (1) uncoated and (2) polydopamine coated-cryogel bioscaffolds.

ii. Compression strength: We determined the compression strength and elastic modulus of bioscaffolds following their immersion in PBS for 1 h using ASTM D695—15 standard.[33] The compressive properties were investigated by applying uniaxial compression (Instron 5565) to bioscaffolds to reduce their original height to 60% under a load cell of 10 kN at the displacement rate of 1–mm min^{-1}. The compressive strength and elastic modulus of bioscaffolds were calculated by plotting a graph of engineering stress (MPa) versus engineering strain (%) according to Eqs. (9) and (10):

$$\sigma = \frac{F}{A_0} \quad (9)$$

$$E = \frac{\sigma_Y}{\varepsilon_Y} \quad (10)$$

where σ is engineering stress (MPa), F is force (N), A_0 is surface area (mm^2) before starting the test, E is elastic modulus (GPa), σ_Y is yield strength (MPa) and ε_Y is yield strain (%). Bioscaffold compressive properties were measured on three separate samples from each of the following experimental groups: (1) uncoated and (2) polydopamine coated-cryogel bioscaffolds.

Bioscaffold interactions with adipose tissue-derived mesenchymal stem cells (AD-MSCs)

i. **AD-MSCs isolation:** Mouse adipose tissue was obtained from the lower abdomen in male C57BL6 mice at 6–8 weeks of age. Harvested adipose tissue was then washed with sterile PBS, minced with scissors and then digested with 1 mg/ml type I collagenase (Sigma-Aldrich) in serum-free medium at 37°C for 3 h. The digestion was then inactivated with an equal volume of Dulbecco's Modified Eagle's medium (DMEM; Gibco) supplemented with 10% fetal bovine serum (FBS; Invitrogen). All samples were then filtered through a 100 μm mesh filter to remove any debris. The cellular pellets were collected and then re-suspended in DMEM-10% FBS-50 U/ml penicillin-50 μg/ml streptomycin in a humidified incubator at 37°C with 5% carbon dioxide. AD-MSCs from passage number 3–5 were used in our studies.

ii. **AD-MSCs flow cytometric characterization:** Surface marker expression was analyzed by flow cytometry (Guava easyCyte system; Millipore) using the phycoerythrin (PE) conjugated mouse monoclonal antibody against CD105, CD90, and CD34 (Biolegend). Adherent cells were detached by treatment with 0.25% trypsin-EDTA, neutralized with DMEM-10% FBS-50 U/ml penicillin-50 μg/ml streptomycin culture medium and disaggregated into single cells by pipetting. The cells were then incubated with the above antibodies for 40 min at room temperature in the dark, washed twice with PBS, re-suspended with 0.5 ml flow cytometry (FACS) buffer (PBS, 2% FBS, 1% P/S) and then immediately characterized using the Guava easyCyte system.

iii. **AD-MSCs culture:** All assays were carried out on ADMSCs that were either seeded directly into bioscaffolds (direct contact) or incubated with "bioscaffold medium" (indirect contact). For direct contact, bioscaffolds were sterilized by soaking them in 70% ethanol for 0.5 h after which time they were then rinsed three times in sterilized PBS and placed at the bottom of 96-well plates. ADMSCs were then seeded into bioscaffolds, achieving a cell density of 5×10^4 cells/well. For indirect contact, ADMSCs were incubated in complete medium (5×10^4 cells/well) for 24 h to allow attachment. "Bioscaffold medium" was then prepared by incubating a bioscaffold with 2 ml culture medium for 5 days at 37°C; this medium was then added (50 μl/well) to AD-MSCs which were then left to incubate for a further 10 days.

iv. **AD-MSCs viability and proliferation:** The viability of ADMSCs was determined using an MTT (4,5-dimethylthiazol-2-yl)-2,5-diphenyltetrazolium bromide assay. Here, 50 μl of MTT solution (0.5 mg/ml) was added to the complete medium in each well and left to incubate at 37°C for 4 h. Water-soluble MTT is taken up by viable cells and converted to an insoluble formazan. Next, 200 μl of DMSO (to dissolve the formazan) was added to each well and left at 37°C for a further 10 min before the absorbance was measured at 570 nm using a microplate spectrophotometer system - the absorbance directly relates to the number of viable cells present.[34,35] Cell viability was determined using the following equation (Eq. 11):

$$\text{Cell viability} = \frac{OD_{sample}}{OD_{control}} \quad (11)$$

where OD_{sample} is the optical density (absorbance) of AD MSCs (from either direct or indirect contact experiments) and $OD_{control}$ is the optical density (absorbance) of AD-MSCs that were not exposed to any bioscaffolds. MTT assay was performed on three separate samples from each of the following experimental groups: (1) control (AD-MSCs that were cultured in culture plates and not exposed to any bio-scaffolds), (2) uncoated, and (3) polydopamine coated-cryogel bioscaffolds.

AD-MSCs were labeled using Hoechst 33342 (for cell nuclei; Thermofisher Scientific), fluorescein diacetate (FDA; for live cells, Thermofisher Scientific) and propidium iodide (PI; for dead cells, Thermofisher Scientific) as the Live/Dead staining solution. The culture medium was removed and the Live/Dead staining solution [Hoechst 33342 (50 μl/well), FDA (75 μl/well) and PI (75 μl/well)] was added and incubated with AD-MSCs for 20 min at 37°C. At the end of the incubation time, the staining solution was removed and cells were washed three times with PBS. The live cell imaging solution (Thermofisher Scientific) was then added to each well before imaging. Images were acquired with a Zeiss LSM710 Confocal Microscope at a magnification of 20× and figures were created with the FIJI software (ImageJ, GNU General Public License). Live/Dead assay was performed on three separate samples from each of the following experimental groups: (1) control (AD-MSCs that were cultured in culture plates and not exposed to any bioscaffolds), (2) uncoated, and (3) polydopamine coated-cryogel bioscaffolds. Confocal imaging was performed on three separate samples from each of the following experimental groups: (1) control (AD-MSCs that were cultured in culture plates and not exposed to any bioscaffolds), (2) uncoated, and (3) polydopamine coated-cryogel bioscaffolds.

Cell adhesion was visualized with SEM by acquiring images from 3–5 random locations (including the top surface as well as within the surface) within each bioscaffold. Sectioned bioscaffolds were washed three times with PBS, fixed using 4% paraformaldehyde for 0.5 h at room temperature and then dehydrated in graded ethanol solutions (50%, 70%, 90%, and finally 100% absolute ethanol). All bioscaffolds were then dried at room temperature, sectioned, sputter coated with Au-Pd and then analyzed with SEM. Cell adhesion was visualized with SEM on three separate samples from each of the following experimental groups: (1) uncoated and (2) polydopamine coated-cryogel bioscaffolds. SEM images were acquired from five random locations within each sample.

Measurement of AD-MSCs number with a hemocytometer was performed on three separate samples from each of the following experimental groups: (1) control (AD-MSCs that were cultured in culture plates and not exposed to any bioscaffolds), (2) uncoated, and (3) polydopamine coated-cryogel bioscaffolds.

Statistical analysis

All results were expressed as mean ± standard error of the mean. Data were analyzed using an unpaired student's *t* test software (GraphPad QuickCalcs: *t* test calculator) with any differences considered statistically significant when $p < 0.05$.

RESULTS

Bioscaffold porosity and density measurement

Synthesized bioscaffolds measured 10 mm (diameter) × 5 mm (thickness) correlating to a volume of 6.78 ± 0.35 cm^3 with a porosity of 75% ± 3% and density of 0.0395 ± 0.006 mg/mm^3.

Bioscaffold structural and chemical analysis

Micro (μ)-CT images demonstrated the shape and distribution of pores within the 3 D porous structure of bioscaf-folds. The results showed that pore sizes fall into two groups include big pores with the size of 300 ± 50 μm and small pores with the size of 30 ± 10 μm. The uncoatedcryogel bioscaffolds were white in color and retained a 3D architecture throughout its processing. Following the immersion of bioscaffolds into a polydopamine solution, a nanolayer of dopamine was noted containing polydopamine nanoparticles which changed the color of each bioscaffold from white to brown (Fig. 2).

Using XPS, both types of bioscaffold (that is, uncoated and polydopamine coated) showed peaks corresponding to elements of carbon (C) at ~284 eV[36], oxygen (O) at ~284 eV[37] and nitrogen (N) at ~400 eV.[38] Coating bioscaffolds with polydopamine also changed their surface chemical composition (that is, the atomic percentage of C, O, and N) [Fig. 3(a)]. These spectra included a C–C, C=C peak with a binding energy of ~284 eV [Fig. 3(b);][39–41] which is observed in collagen spectra.[42] The atomic structure of collagen (that is, the material of our bioscaffolds) was confirmed with its three characteristic footprint signatures at 1630 cm^{-1} (corresponding to the amide I due to carbonyl stretching—C–H), 1551 cm^{-1} (corresponding to the amide II due to vibrations on the plane of the N–H bond and C–N stretching) and 1232 cm^{-1} (corresponding to vibrations on the plane of amide III due to C–N stretching and N–H deformation). Upon crosslinking of collagen, amide A (3309 cm^{-1}) and amide B (2930 cm^{-1}) spectral signatures were also noted. The peaks identified at 1454 cm^{-1} and between 1417 and 1360 cm^{-1}, correspond to the stereochemistry of pyrrolidine rings of proline and hydroxyproline. The peaks found between 3100 and 3400 cm^{-1} occur due to O–H and N–H stretching of amide A. No additional bands related to the polydopamine coating were observed [Fig. 3(c)]. The Raman spectral signal at 2670 cm^{-1} demonstrated the successful introduction of the thiol group onto the surface of bioscaffolds. Two broad peaks at ~1370 and 1630 cm^{-1} correspond to vibrations of catechol moieties after the polydopamine coating [Fig. 3(d)].

Bioscaffold water uptake, swelling, and biodegradability

Both types of bioscaffold demonstrated the ability to uptake water over three successive immersions in water. However, within first 30 s of each of the three immersion cycles, the percent of water uptake was significantly greater in uncoated-cryogel bioscaffolds when

compared to the polydopamine coated-cryogel bioscaffolds. For example, following the first immersion, uncoated-cryogel bioscaffolds demonstrated a 62% ± 5% water uptake compared to the polydopamine coated-cryogel bioscaffolds at 21% ± 3% [Fig. 4(a), $p < 0.05$]. Moreover, the average swelling ratio was significantly reduced in polydopamine coated-cryogel bioscaf-folds when compared to uncoated-cryogel bioscaffolds (4.5 ± 0.5 vs. 23.4 ± 1.5 swelling ratio; [Fig. 4(b)], $p < 0.05$). Both bioscaffolds showed biodegradation following incubation with PBS, however, polydopamine coated-cryogel bio-scaffolds degraded slower compared to uncoated-cryogel bioscaffolds. For example, at 1 week, uncoated-cryogel bio-scaffolds had been degraded by 17.5% ± 2% whereas polydopamine coated-cryogel bioscaffolds only degraded by 5.45% ± 0.5% [Fig. 4(c), $p < 0.05$]. Moreover, compared to the SEM morphology of polydopamine coated-cryogel bio-scaffolds [Fig. 4(d)], the hydration-dehydration process with water did not change the bioscaffold morphology [Fig. 4(e)].

Bioscaffold rheological and mechanical properties

Both types of bioscaffold also displayed a normal gel-like viscoelastic response over the whole frequency range. The G', as an indicator of bioscaffold stiffness, was 10–14 times higher than the G'' indicating the formation of solid gels. Both moduli showed very little frequency dependence (particularly at low frequencies), meaning that viscoelastic properties of bioscaffolds are dominated by the established network structure. Moreover, both types of bioscaffold displayed liquid-like viscous behavior ($G' < G''$) at oscillation strains higher than 100% (uncoated-cryogel bioscaffolds) and 250% (polydopamine coated-cryogel bioscaffolds), respectively. Both types of bioscaffold also showed shear thinning and a subsequent quick recovery of their individual elastic properties after shearing had ended. The G' of uncoated-cryogel bioscaffolds changed from 430 ± 15 to 519 ± 20 over the ω range of 0.1–100 rad/s [Fig. 5(a)], from 428 ± 20 to 4 ± 1 over the γ range of 1000%–1% [Fig. 5(b)] and from 445 ± 15 to 449 ± 15 Pa [Fig. 5(c)] over the ts range of 12–300 s. The addition of polydopamine coating to bioscaffolds resulted in a significant increase in G' over the ω range (846 ± 45 to 977 ± 50 Pa vs. 430 ± 15 to 519 ± 20 Pa; [Fig. 5(d)], $p < 0.05$), the γ range (891 ± 35 to 10 ± 2 Pa vs. 428 ± 20 to 4 ± 1 Pa; [Fig. 5(e)], $p < 0.05$) and the ts range (715 ± 25 to 730 ± 20 Pa vs. 445 ± 15 to 449 ± 15 Pa; [Fig. 5(f)], $p < 0.05$). Also, the cross linking density of our bioscaffolds obtained 0.19 ± 0.04 mol Pa/J.

Both types of bioscaffold showed elastic behavior till 40% compression of their length. Thereafter, the uni-axial stress was transferred to the plastic region. Uncoatedcryogel bioscaffolds showed an elastic modulus of 3.6 ± 0 KPa, yield strength of 1.45 ± 0.11 KPa and compression strength of 1.75 ± 0.13 KPa [Fig. 5(g)]. The addition of polydopamine coating to bioscaffolds resulted in a significant increase in elastic modulus (9.6 ± 0.35 vs. 3.6 ± 0.2 KPa; $p < 0.05$), yield strength (2.7 ± 0.23 vs. 1.45 ± 0.11 KPa; $p < 0.05$) and compression strength (4.1 ± 0.35 vs. 1.75 ± 0.13 KPa; $p < 0.05$). Moreover, both uncoated and polydopamine coated-cryogel bioscaffolds showed recovery to their original shape after removing the load in compression test [Fig. 5(h)].

Bioscaffold interactions with adipose tissue-derived mesenchymal stem cells (AD-MSCs)

Analysis of surface antigen expression showed that ADMSCs expressed CD105 and CD90 markers (positive, [Fig. 6(a–d)]) with no expression of the CD34 marker (negative, [Fig. 6(e,f)]). Relative to the control group (AD-MSCs cultured in traditional cell culture plates), there was a significantly greater viability of AD-MSCs when they were seeded into bioscaffolds. The results of MTT [Fig. 7(a–c)] and Live/Dead assays [Fig. 7(d–f)] from both direct [Fig. 7(a,b,d,e)] and indirect [Fig. 7(c,f)] cell culture methods at day 1 [Fig. 7(a,d)] and 10 [Fig. 7(b,c,e,f)] showed that AD-MSCs seeded into polydopamine coated-cryogel bioscaffolds had a higher viability compared to uncoated-cryogel bioscaffolds and the control group. For example, according to results obtained from the MTT assay at day 1, AD-MSCs seeded into uncoated-cryogel bioscaffolds demonstrated a 0.55 ± 0.12-fold increase in the cell viability compared to the control group. However, the addition of a polydopamine coating to bioscaffolds resulted in a significant increase in cell viability (2.40 ± 0.05 vs. 0.55 ± 0.12; [Fig. 7(a)], $p < 0.05$). According to results obtained from the Live/Dead assay at day 1, the percentage of live AD-MSCs in uncoated-cryogel bioscaffolds was 75% ± 6%. However, the addition of polydopamine coating to bioscaffolds resulted in a significant increase in the percentage of live cells (90% ± 6% vs. 75% ± 6%; [Fig. 7(d)], $p < 0.05$).

SEM images showed the morphology of seeded AD-MSCs into bioscaffolds with cells having a long and thin morphology with widely dispersed filopodia and flattened polygonal extensions on the superficial layer and within the center of both bioscaffolds. The SEM images related to polydopamine coated-cryogel bioscaffolds shows an increase in density of AD-MSCs compared to uncoated-cryogel bioscaffolds. Also, the SEM images from the center of bioscaffolds show the cell distribution through the bioscaffold thickness and inside individual pores. Moreover, the cell density increased with culture time from 1 to 10 days (Fig. 8).

Confocal images showed that AD-MSCs seeded into bio-scaffolds were higher in number [Fig. 9(b,c,e,f,h,i)] compared to AD-MSCs cultured alone in a traditional cell culture plate (control group; [Fig. 9(a,d,g)], $p < 0.05$). These results suggest that AD-MSCs were able to proliferate into bioscaffolds, with a significantly higher degree of proliferation demonstrated in polydopamine coated-cryogel bioscaf-folds [Fig. 9(c,f)] at day 1 [Fig. 9(c)] and day 10 [Fig. 9(f)] compared to AD-MSCs cultured in uncoated-cryogel bioscaf-folds [Fig. 9(b,e), $p < 0.05$]. Moreover, AD-MSCs were distributed evenly within the pores of bioscaffolds as well as attached to the surface as has been indicated by white arrows [Fig. 9(b,c,e,f)]. AD-MSCs counting using a hemocytometer at day 1 and 10 showed that AD-MSCs cultured alone in a traditional cell culture plate (control group) enhanced the cell proliferation and AD-MSCs seeded into bioscaffolds resulted in a higher proliferation compared to the control group. However, AD-MSCs seeded into polydopamine coated-cryogel bioscaffolds demonstrated a higher amount of proliferation compared to AD-MSCs seeded into uncoated-cryogel bioscaffolds [Fig. 9(j), $p < 0.05$]. For example, 50,000 AD-MSCs were initially used for each experimental group at day 1; by day 10 the number of AD-MSCs seeded into the uncoated and polydopamine coated-cryogel bioscaffolds were 400,000 ± 50,000 and 600,000 ± 70,000, respectively, which was significantly higher than the control group (i.e., 270,000 ± 30,000, $p < 0.05$). Together, these results suggested that AD-MSCs were capable

of proliferating more in bioscaffolds, and especially in polydopamine coated-cryogel bioscaffolds, when compared to the control group.

DISCUSSION

Collagen is a major ECM component which can facilitate cell growth.[43] The widespread use of collagen is due to its desirable biocompatibility, mechanical properties and biodegradability.[44,45] Indeed, collagen provides a suitable “base-biomaterial” for the fabrication of porous 3D bioscaffolds which can be used for tissue engineering across numerous applications.[46,47] The 3D platform of bioscaffolds also provide a significant advantage over conventional 2D culture plates for cellular interactions and growth. Studies have shown that the pore size of bioscaffolds is crucial for determining their function, with smaller pores providing better nutrient and oxygen transfer to facilitate cell growth and proliferation, while large pores provide a high surface area to accommodate cells.[48] Bioscaffolds with a larger mean pore sizes (i.e., 300 mm) have also been shown to be associated with a significantly higher cell viability and proliferation relative to bioscaffolds with a smaller mean pore size.[49] In keeping with these studies, structural analysis of our collagen bioscaffold demonstrated it to have a mean pore size of 300 6 100 mm, which we have shown facilitates AD-MSCs viability and proliferation, especially when compared to AD-MSCs cultured on conventional 2D culture plates. In addition, our bioscaffold has small pores (30 ± 10 μm). The small pores will help promote blood vessel ingrowth into the bioscaffold, as supported by recent reports which have shown that pore sizes between 30–40 mm facilitates vascularization of implantable bioscaf-folds.[50,51] Our bioscaffold also has a high degree of porosity (75% ± 3%) with a corresponding high swelling ratio.[48] The high porosity and interconnected macropores of our bioscaf-fold creates a physical space to facilitate cell movement and distribution throughout the bioscaffold. In turn, this is advantageous for nutrient and oxygen transfer to all cells seeded into the bioscaffold while also preventing cell loss from cellular overcrowding, which commonly occurs when using traditional cell culture plates.[5] Once inside bioscaf-folds, cells have a substrate to which they can adhere to and proliferate on while also interacting with their surrounding environment in all three dimensions, similar to how they would interact *in vivo*.[52]

Many surface coating strategies have been previously reported for the improvement of cellular function on bio-scaffolds.[53–55] Dopamine undergoes oxidative polymerization in alkaline conditions and has a strong adsorption onto a wide variety of substrates through covalent bonding and strong intermolecular interactions.[18,56] Polydopamine coatings can therefore act as a strong anchor between cells and substrates.[16,19–21] Although polydopamine can be produced in a facile and simple polymerization process, its formation mechanism is heavily debated owing to the complexity of the reactions of 5,6-dihydroxyindole, the final oxidation product of dopamine, and other catecholamines can undergo under different experimental conditions.[17] However, polydopamine has been shown to reduce the *in vivo* toxicity of bioscaffolds and has been shown to improve cell behavior on various substrates.[53–55,57] For these reasons, we coated our collagen based cryogel bioscaffold with polydopamine. Following coating the cryogel bioscaffolds with polydopamine, we observed formation of a polydopamine nanolayer which contains polydopamine nanoparticles. Similarly, Lee et al.[16] reported the method of dip-coating

materials in an aqueous solution of dopamine and found a similar nano-structured polydopamine coating formed on a wide range of different substrates including noble metals, oxides, semiconductors, ceramics, and synthetic polymers. Nanostructured coatings are an effective surface modification method to improve the biocompatibility of biomaterials.[58] Recently, polydopamine nanoparticles have been studied in the bio-materials field.[59] Some studies have revealed that polydopamine nanoparticle-coated substrates promote cell behavior and tissue ingrowth due to the nanostructures and cell affinity of the polydopamine nanoparticles. Wang et al.[60] also used polydopamine nanoparticles, and demonstrated that the polydopamine nanoparticles provided multiple bio-active sites for the adsorption of proteins and peptides, while improving the adhesion of bone marrow stromal cells compared to pristine polydopamine coated substrates.

The water uptake and swelling of both uncoated and polydopamine-coated bioscaffolds allowed cells to infiltrate into the bioscaffold as demonstrated in SEM cross-sectional images of bioscaffolds (Fig. 8). However, the decrease in percentage of water uptake and swelling ratio of polydopamine coated-cryogel bioscaffolds compared to uncoated bioscaffolds, results in an increased stability. This translates to bioscaffolds experiencing less volume change when exposed to aqueous environments,[61,62] which will reduce the stress and damage to any cells seeded on their surface. Our results also showed that polydopamine coating decreases the degree of bioscaffold bio-degradation when compared to uncoated-cryogel bioscaffolds, likely due to its reduced water uptake. This is advantageous since a faster rate of bioscaffold biodegradation would result in its shrinkage and loss of interconnectivity which, in turn, would limit cell growth, migration and nutrient flow.[63,64] Finally, the polydopamine coating also increased the strength of cryogel bioscaffolds, as evidenced by the results of compression test, which is important for the bioscaffold to protect its cellular cargo during storage and transportation.[65]

In addition, our results show that the collagen bioscaf-folds are soft and compliable given that they can be compressed to a fraction of their original volume before returning to their original shape—properties which have been previously shown to promote cellular proliferation.[65] The rheological behavior of our bioscaffolds changed following coating with polydopamine which can be due to the water content of our bioscaffolds. Prior to rheological testing, our samples were immersed in PBS. Given that uncoated cryogel bioscaffolds had a different water uptake capacity compared to polydopamine coated-cryogel bioscaf-folds (Fig. 4), the rheological behavior of our cryogel bio-scaffold will therefore vary following polydopamine coating. Previous research has also shown that when free water goes into polymeric structures, it can influence gelation processes and therefore the rheological behavior of the polymer.[66] Furthermore, when hydrogels are saturated in PBS, their bulk rheology changes with them now demonstrating a substantial elastic response with an increase in both the storage and loss modulus compared to non-saturated hydrogels. Taken together, the rheological behavior results of our bioscaffolds will depend on their water content following PBS saturation. Our bioscaffolds have been designed to potentially be used as a platform for the co-transplantation of AD-MSCs and pancreatic islets. Potential pre-clinical and clinical sites of implantation of our bioscaffold include the subcutaneous skin, mesentry or omentum. Therefore, compression loads will be expected to be applied to our bioscaffold. Based on the results of compression tests, our bioscaffolds showed recovery

to their original shape following removal of compressive stresses, thus showing their elasticity under compressive loads. Our rheological and mechanical studies have shown that polydopamine coated-cryogel bioscaffolds are more elastic when compared to uncoated cryogel bioscaffolds. Previous studies have also shown that incorporation of polydopamine increases the mechanical strength of biomaterials including collagen.[67] For example, Hu and colleagues[68] have shown that when dopamine is incorporated into the collagen, it increases both its tensile strength and elongation at break. Furthermore, since our rheological and mechanical tests have been performed in the wet state, the improvement in the properties of collagen could be related to an effect of interfacial interactions of polydopamine with water. From the results of water uptake and swelling, we have shown that polydopamine coating decreases the tendency of the surface to be wetted by water. Hence, we expect that there will be a lower amount of water diffusing into the structure of polydopamine coated-cryogel bioscaffolds, which can also be another reason for the higher rheological and mechanical properties of polydopamine coated-cryogel bioscaffolds compared to those seen in uncoated cryogel bioscaffolds. Moreover, polydopamine could also fill into some of the pores of the collagen bioscaffold, especially since we found that the porosity of polydopamine coated cryogel bioscaf-folds was less than that of the uncoated cryogel bioscaffolds. Following polydopamine coating, the porosity decreased from 75% ± 3% to 70% ± 2%, which may be another reason that the mechanical strength after coating with polydopamine was enhanced since the porosity can decrease the compressive properties.[69]

Our results demonstrated an increased adhesion, viability and proliferation of AD-MSCs when they were seeded into polydopamine coated cryogel bioscaffolds when compared to uncoated bioscaffolds. Similar effects of polydopamine have also been reported by Rim and colleagues who analyzed the effect of polydopamine coated-poly(L-lactide) electrospun fibers on human MSCs (hMSCs). These studies concluded that the relative viability of cells cultured on polydopamine coated-fibers was double that of the uncoated fibers and that the coated fibers also supported the proliferation of hMSCs.[70] Prior studies have also suggested that cell adhesion and growth can be enhanced by free amine groups of polydopamine since amine groups confer hydrophilicity and positive charge to substrates.[71,72] Another explanation for the improved viability and proliferation of AD-MSC on polydopamine coated bioscaffolds could also be due to their ability to grow more efficiently when they are within a microenvironment with high elasticity.[73] Studies have shown that the elasticity of the tissue matrix which surrounds MSCs is important for their function.[74,75] Our rheological studies have shown that polydopamine coated bioscaffold are indeed more elastic when compared to uncoated cryogel bioscaffolds. Furthermore, the elastic properties of polydopamine coated-cryogel bioscaffolds are maintained, even when they are subjected to different oscillation strains (i.e., 0.1%–1000%).

As a major component of naturally occurring melanin that is widely distributed in human body, polydopamine shows excellent biocompatibility.[76] Previous research show that substrates coated with polydopamine can significantly improve cell affinity and promote cell behavior compared with uncoated substrates.[77] The adhesion of fibroblasts and megakaryocytes (bone marrow cells) to polydopamine coated surfaces has been evaluated by Lee et al.[16] Fibroblast cell adhesion was supported on polydopamine coated surfaces as well as on unmodified controls, while limited megakaryocytic adhesion was seen on

polydopamine coating. These observations showed that the cytocompatibility of the polydopamine coatings seems cell type-dependent. Furthermore, the polydopamine coating has been shown to be a powerful route for converting a variety of bioinert substrates into bioactive ones, including non-wetting surfaces[78] and bioscaffolds,[19] which promote cell adhesion of several cell types, such as osteoblast, pheochromocytoma, and chondrocytes. The possible mechanism for the enhancement of cell adhesion by the polydopamine coatings have also been investigated.[19,78] Ku and colleagues[78] found that serum protein adsorption occurred on both uncoated and polydopamine-coated substrates, and they therefore hypothesized that the polydopamine coating potentially prevent possible protein denaturation, which is responsible for enhanced cell adhesion. Tsai and colleagues[19] compared cell adhesion on polydopamine-coated surfaces under serum-containing and serum-free conditions and found that cell adhesion onto polydopamine-coated surfaces was significantly higher in the presence of serum proteins. Since fibronectin adsorption was also higher on polydopamine-coated surfaces than uncoated surfaces they suggested that the enhancement of cell adhesion to polydopamine-coated surfaces is likely due to enhanced immobilization and/or adsorption of adhesive proteins such as fibronectin on the surface of substrates.

The polydopamine coating in our study enhanced ADMSCs viability and proliferation, which could be ascribed to two reasons. The first reason is the intrinsic cell affinity of polydopamine. Cho et al.[79] reported that polydopamine coating of the surface of polyethylene glycol adipate and polystyrene substrates could promote the proliferation and spreading of human neural stem cells. She et al.[80] reported that polydopamine coating of polylactic acid scaffold surfaces increased the adhesion, proliferation, and differentiation of human AD-MSCs. Polydopamine can adsorb ECM proteins, such as fibronectin and collagen, providing a favorable environment for cell proliferation and spreading.[81] The second reason is the nanostructure produced by our polydopamine nanolayer and nanoparticles. It should be noted that most of the previous studies focused on dense polydopamine films,[82] however, in this study, the polydopamine coating contained polydopamine nanoparticles which facilitates cell adhesion. It is commonly accepted that nanostructures can improve the adsorption of ECM biomolecules, which can enhance the cellular adhesion of the coatings.[83]

Future studies using our bioscaffold will investigate the beneficial effect of our 3D construct with other cells lines including human AD-MSCs and human bone marrow MSCs (BM-MSCs). Furthermore, both vascular endothelial growth factor-A (VEGF-A) and hepatocyte growth factor-1 (HGF-1) are angiogenic factors which have been shown to regulate neovascularization, improve tissue blood perfusion and induce mature blood vessel network formation, thereby helping in organ and cellular transplantation.[84–86] As poly-dopamine has repeating 3,4-dihydroxy-L-phenylalaninelysine (DOPA-K) motifs, it has strong adsorption through covalent bonding and intermolecular interactions.[30] Hence, our polydopamine coating could serve as the interface to enable our bioscaffold to be functionalized with VEGF and HGF-1, especially since these angiogenic growth factors can be immobilized on the surface of polydopamine by simple dipping.[87] Hence, future experiments will explore the functionalization of our polydopamine coated-cryogel bio-scaffolds with VEGF and HGF-1, which we hypothesize that this will help promote angiogenesis and blood vessel

growth into our bioscaffold, thereby opening up possibilities for the engraftment of our bioscaffold into living subjects. In the future, we also plan to seed our cryogel bioscaffold with native proteins that elicit cell growth. The resulting attachment, viability, proliferation, and cell infiltration will then be compared between uncoated and polydopamine-coated bioscaffolds.

CONCLUSION

Collagen based cryogel bioscaffolds with 75% ± 3% porosity and 300 ± 100 μm pore size were synthesized and coated with polydopamine. The results from the present study demonstrate that coating the macroporous cryogel bioscaf-folds with polydopamine decreases their water uptake (41% ± 5%), swelling (81% ± 10%) and degree of biodegradation (12% ± 3%) while increasing their stiffness (48% ± 2%) and compressive strength (57% ± 5%) when compared to uncoated-cryogel bioscaffolds. Seeding AD-MSCs into polydopamine coated-cryogel bioscaffolds increased their viability (52% ± 4%) and proliferation (33% ± 3%) when compared to AD-MSCs cultured on uncoated-cryogel bioscaffolds. In summary, our results show the potential for polydopamine coated-cryogel bioscaffolds in regenerative medicine as an efficient, low-cost storing and transporting matrix for AD-MSCs. Furthermore, our bioscaffold can be easily modified with additional functional coatings to support its use in different indications.

ACKNOWLEDGMENTS

This work was supported by Stanford Nano Shared Facilities (SNSF) grant (1161726–146-DAARZ), as part of the grant supported by the National Science Foundation grant (ECCS-1542152), and the Stanford Neuroscience Microscopy Service grant (NIH NS069375).

Contract grant sponsor:Stanford Nano Shared Facilities (SNSF); contract grant number: 1161726–146-DAARZ

Contract grant sponsor: National Science Foundation; contract grant number: ECCS-1542152

Contract grant sponsor:Stanford Neuroscience Microscopy Service; contract grant number: NIH NS069375

REFERENCESS

1. Nolan K, Millet Y, Ricordi C, Stabler CL. Tissue engineering and biomaterials in regenerative medicine. Cell Transplant 2008;17: 241–243. [PubMed: 18522227]
2. Saul JM, Williams DF. Hydrogels in regenerative medicine. Handb Polym Appl Med Med Devices 2013; 279–302. doi:10.1016/B978-0-323-22805-3.00012-8.
3. Dubruel P, Unger R, Van Vlierberghe S, Cnudde V, Jacobs PJS, Schacht E, Kirkpatrick CJ. Porous gelatin hydrogels: 2. In vitro cell interaction study. Biomacromolecules 2007;8:338–344. () doi: 10.1021/bm0606869. [PubMed: 17291056]
4. Gun'ko VM, Savina IN, Mikhalovsky SV. Cryogels: Morphological, structural and adsorption characterisation. Adv Colloid Interface Sci 2013;187–188:1–46. doi:10.1016/j.cis.2012.11.001.
5. Bencherif SA, Warren Sands R, Ali OA, Li WA, Lewin SA, Braschler TM, Shih T-Y, Verbeke CS, Bhatta D, Dranoff G, Mooney DJ. Injectable cryogel-based whole-cell cancer vaccines. Nat Commun 2015;6:7556. doi:10.1038/ncomms8556. [PubMed: 26265369]
6. Jain E, Kumar A. Designing supermacroporous cryogels based on polyacrylonitrile and a polyacrylamide-chitosan semi-interpenetrating network. J Biomater Sci Polym Ed 2009;20:877–902. doi: 10.1163/156856209X444321. [PubMed: 19454158]

7. Koshy ST, Ferrante TC, Lewin SA, Mooney DJ. Injectable, porous, and cell-responsive gelatin cryogels. Biomaterials 2014;35:2477–2487. doi:10.1016/j.biomaterials.2013.11.044. [PubMed: 24345735]
8. Bhat S, Kumar A. Cell proliferation on three-dimensional chitosanagarose-gelatin cryogel scaffolds for tissue engineering applications. J Biosci Bioeng 2012;114:663–670. doi:10.1016/j.jbiosc.2012.07.005. [PubMed: 22884715]
9. Lee CH, Singla A, Lee Y. Biomedical applications of collagen. Int J Pharm 2001;221:1–22. doi:10.1016/S0378-5173(01)00691-3. [PubMed: 11397563]
10. Rodrigues SC, Salgado CL, Sahu A, Garcia MP, Fernandes MH, Monteiro FJ. Preparation and characterization of collagen-nanohydroxyapatite biocomposite scaffolds by cryogelation method for bone tissue engineering applications. J Biomed Mater Res A 2013;101A:1080–1094. doi:10.1002/jbm.a.34394.
11. Hirata E, Uo M, Takita H, Akasaka T, Watari F, Yokoyama A. Development of a 3D collagen scaffold coated with multiwalled carbon nanotubes. J Biomed Mater Res B Appl Biomater 2009;90B:629–634. doi:10.1002/jbm.b.31327.
12. Yang HS, La W-G, Bhang SH, Lee T-J, Lee M, Kim B-S. Apatite-coated collagen scaffold for bone morphogenetic protein-2 delivery. Tissue Eng A 2011;17:2153–2164. doi:10.1089/ten.tea.2010.0702.
13. Ibara A, Miyaji H, Fugetsu B, Nishida E, Takita H, Tanaka S, Sugaya T, Kawanami M. Osteoconductivity and biodegradability of collagen scaffold coated with nano-β-TCP and fibroblast growth factor 2. J Nanomater 2013;2013:1.
14. Ye Q, Zhou F, Liu W. Bioinspired catecholic chemistry for surface modification. Chem Soc Rev 2011;40:4244. doi:10.1039/c1cs15026j. [PubMed: 21603689]
15. Huang S, Liang N, Hu Y, Zhou X, Abidi N. Polydopamine-assisted surface modification for bone biosubstitutes. Biomed Res Int 2016;2016:1. doi:10.1155/2016/2389895.
16. Lee H, Dellatore SM, Miller WM, Messersmith PB. Mussel-inspired surface chemistry for multifunctional coatings. Science 2007;318: 426–430. doi:10.1126/science.1147241. [PubMed: 17947576]
17. Liu Y, Ai K, Lu L. Polydopamine and its derivative materials: Synthesis and promising applications in energy, environmental, and biomedical fields. Chem Rev 2014;114:5057–5115. doi:10.1021/cr400407a. [PubMed: 24517847]
18. Yang F, Zhao B. Adhesion properties of self-polymerized dopa-mine thin film. Open Surf Sci J 2011;3:115–122. doi:10.2174/1876531901103010115.
19. Tsai WB, Chen WT, Chien HW, Kuo WH, Wang MJ. Poly(dopamine) coating of scaffolds for articular cartilage tissue engineering. Acta Biomater 2011;7:4187–4194. doi:10.1016/j.actbio.2011.07.024. [PubMed: 21839186]
20. Ko E, Yang K, Shin J, Cho SW. Polydopamine-assisted osteoinductive peptide immobilization of polymer scaffolds for enhanced bone regeneration by human adipose-derived stem cells. Biomacromolecules 2013;14:3202–3213. doi:10.1021/bm4008343. [PubMed: 23941596]
21. Tsai WB, Chen WT, Chien HW, Kuo WH, Wang MJ. Poly(dopamine) coating to biodegradable polymers for bone tissue engineering. J Biomater Appl 2014;28:837–848. doi:10.1177/0885328213483842. [PubMed: 24381201]
22. Chuah YJ, Koh YT, Lim K, Menon NV, Wu Y, Kang Y. Simple surface engineering of polydimethylsiloxane with polydopamine for stabilized mesenchymal stem cell adhesion and multipotency. Sci Rep 2016;5:18162. doi:10.1038/srep18162.
23. Bhat S, Kumar A. Biomaterials in regenerative medicine. J Postgr Med Edu Res 2012;46:81–89.
24. El-Badawy A, Amer M, Abdelbaset R, Sherif SN, Abo-Elela M, Ghallab YH, Abdelhamid H, Ismail Y, El-Badri N. Adipose stem cells display higher regenerative capacities and more adaptable electro-kinetic properties compared to bone marrow-derived mesenchymal stromal cells. Sci Rep 2016;6. doi:10.1038/srep37801. [PubMed: 28442741]
25. Via AG, Frizziero A, Oliva F. Biological properties of mesenchymal stem cells from different sources. Muscles Ligaments Tendons J 2012;2:154–162. [PubMed: 23738292]
26. Caplan AI. Adult mesenchymal stem cells for tissue engineering versus regenerative medicine. J Cell Physiol 2007;213:341–347. doi:10.1002/jcp.21200. [PubMed: 17620285]

27. Seru P Madsen OD Mandrup-Poulsen T, Islet and stem cell transplantation for treating diabetes. Bmj 2001;322:29–32. doi: 10.1136/bmj.333.7563.334. [PubMed: 11141151]
28. Krishnan R, Alexander M, Robles L, Foster CE, Lakey JRT. Islet and stem cell encapsulation for clinical transplantation. Rev Diabet Stud 2014;11:84–101. doi:10.1900/RDS.2014.11.84. [PubMed: 25148368]
29. Ito T, Itakura S, Todorov I, Rawson J, Asari S, Shintaku J, Nair I, Ferreri K, Kandeel F, Mullen Y. Mesenchymal stem cell and islet co transplantation promotes graft revascularization and function. Transplantation 2010;89:1438–1445. doi:10.1097/TP.0b013e3181db09c4. [PubMed: 20568673]
30. He S, Zhou P, Wang L, Xiong X, Zhang Y, Deng Y, Wei S. Antibiotic-decorated titanium with enhanced antibacterial activity through adhesive polydopamine for dental/bone implant. J R Soc Interface 2014;11:20140169–20140169. doi:10.1098/rsif.2014.0169. [PubMed: 24647910]
31. Sharma A, Bhat S, Vishnoi T, Nayak V, Kumar A. Three-dimensional supermacroporous carrageenan-gelatin cryogel matrix for tissue engineering applications. Biomed Res. Int 2013;2013:1. doi: 10.1155/2013/478279.
32. Raina DB, Koul R, Bangroo A, Kumar A. Fabrication temperature modulates bulk properties of polymeric gels synthesized by different crosslinking methods. RSC Adv 2014;4:31855–31873. doi: 10.1039/c4ra05547k.
33. ASTM International, Standard test method for compressive properties of rigid plastics D695–15. Ann B ASTM Stand 2008: 1–8. doi: 10.1520/D0695-15.2.
34. Pariente J-L, Kim B-S, Atala A. In vitro biocompatibility evaluation of naturally derived and synthetic biomaterials using normal human bladder smooth muscle cells. J Urol 2002;167:1867–1871. doi:10.1016/S0022-5347(05)65251-2. [PubMed: 11912450]
35. Song E, Yeon Kim S, Chun T, Byun HJ, Lee YM. Collagen scaffolds derived from a marine source and their biocompatibility. Biomaterials 2006;27:2951–2961. doi:10.1016/j.biomaterials.2006.01.015. [PubMed: 16457878]
36. Yang S, Dong J, Yao Z, Shen C, Shi X, Tian Y, Lin S, Zhang X. One-pot synthesis of graphene-supported monodisperse pd nano-particles as catalyst for formic acid electro-oxidation. Sci Rep 2015;4: doi:10.1038/srep04501.
37. Zhang J, Gao D, Yang G, Zhang J, Shi Z, Zhang Z, Zhu Z, Xue D. Synthesis and magnetic properties of Zr doped Zno nanoparticles. Nanoscale Res Lett 2011;6:587–521. ()doi: 10.1186/1556-276X-6–587. [PubMed: 22074396]
38. Sen Li J, Li SL, Tang YJ, Li K, Zhou L, Kong N, Lan YQ, Bao JC, Dai ZH. Heteroatoms ternary-doped porous carbons derived from MOFs as metal-free electrocatalysts for oxygen reduction reaction. Sci Rep 2015;4. doi:10.1038/srep05130.
39. Ju J, Zhang R, He S, Chen W. Nitrogen-doped graphene quantum dots-based fluorescent probe for the sensitive turn-on detection of glutathione and its cellular imaging. RSC Adv 2014;4:52583–52589. doi:10.1039/C4RA10601F.
40. Gong P, Hou K, Ye X, Ma L, Wang J, Yang S. Synthesis of highly luminescent fluorinated graphene quantum dots with tunable fluorine coverage and size. Mater Lett 2015;143:112–115. doi: 10.1016/j.matlet.2014.12.058.
41. Permatasari FA, Aimon AH, Iskandar F, Ogi T, Okuyama K. Role of C–N configurations in the photoluminescence of graphene quantum dots synthesized by a hydrothermal route. Sci Rep 2016;6. doi:10.1038/srep21042.
42. Thanikaivelan P, Narayanan NT, Pradhan BK, Ajayan PM. Collagen based magnetic nanocomposites for oil removal applications. Sci Rep 2012;2. doi:10.1038/srep00230.
43. Chan EC, Kuo SM, Kong AM, Morrison WA, Dusting GJ, Mitchell GM, Lim SY, Liu GS. Three dimensional collagen scaffold promotes intrinsic vascularisation for tissue engineering applications. PLoS One 2016;11:e0149799. doi:10.1371/journal.pone.0149799. [PubMed: 26900837]
44. Yannas IV, Tzeranis DS, Harley BA, So PTC. Biologically active collagen-based scaffolds: advances in processing and characterization. Philos Trans R Soc A Math Phys Eng Sci 2010;368:2123–2139. doi:10.1098/rsta.2010.0015.

45. Abou Neel EA, Bozec L, Knowles JC, Syed O, Mudera V, Day R, Hyun JK. Collagen – Emerging collagen based therapies hit the patient. Adv Drug Deliv Rev 2013;65:429–456. doi:10.1016/j.addr.2012.08.010. [PubMed: 22960357]
46. Glowacki J, Mizuno S. Collagen scaffolds for tissue engineering. Biopolymers 2008;89:338–344. doi:10.1002/bip.20871. [PubMed: 17941007]
47. Roelofs LAJ, Eggink AJ, Hulsbergen-Van De Kaa CA, Wijnen RMH, Van Kuppevelt TH, Van Moerkerk HTB, Crevels AJ, Hanssen A, Lotgering FK, Van Den Berg PP, Feitz WFJ. Fetal bladder wall regeneration with a collagen biomatrix and histological evaluation of bladder exstrophy in a fetal sheep model. Fetal Diagn Ther 2008;24:7–14. doi:10.1159/000132399. [PubMed: 18504374]
48. Kumari J, Karande AA, Kumar A. Combined effect of cryogel matrix and temperature-reversible soluble-insoluble polymer for the development of in vitro human liver tissue. ACS Appl Mater Interfaces 2016;8:264–277. doi:10.1021/acsami.5b08607. [PubMed: 26654271]
49. Matsiko A, Gleeson JP, O'Brien FJ. Scaffold mean pore size influences mesenchymal stem cell chondrogenic differentiation and matrix deposition. Tissue Eng A 2015;21:486–497. doi:10.1089/ten.tea.2013.0545.
50. Madden LR, Mortisen DJ, Sussman EM, Dupras SK, Fugate JA, Cuy JL, Hauch KD, Laflamme MA, Murry CE, Ratner BD. Proangiogenic scaffolds as functional templates for cardiac tissue engineering. Proc Natl Acad Sci 2010;107:15211–15216. doi:10.1073/pnas.1006442107. [PubMed: 20696917]
51. Buitinga M, Assen F, Hanegraaf M, Wieringa P, Hilderink J, Moroni L, Truckenmüller R, van Blitterswijk C, Römer GW, Carlotti F, de Koning E, Karperien M, van Apeldoorn A. Micro-fabricated scaffolds lead to efficient remission of diabetes in mice. Biomaterials 2017;135:10–22. doi:10.1016/j.biomaterials.2017.03.031. [PubMed: 28478326]
52. Mandal BB, Kundu SC. Cell proliferation and migration in silk fibroin 3D scaffolds. Biomaterials 2009;30:2956–2965. doi:10.1016/j.biomaterials.2009.02.006. [PubMed: 19249094]
53. Yoo HS, Kim TG, Park TG. Surface-functionalized electrospun nanofibers for tissue engineering and drug delivery. Adv Drug Deliv Rev 2009;61:1033–1042. doi:10.1016/j.addr.2009.07.007. [PubMed: 19643152]
54. Martins A, Pinho ED, Faria S, Pashkuleva I, Marques AP, Reis RL, Neves NM. Surface modification of electrospun polycaprolactone nanofiber meshes by plasma treatment to enhance biological performance. Small 2009;5:1206. doi:10.1002/smll.200801648.
55. Ma Z, Gao C, Gong Y, Shen J. Cartilage tissue engineering PLLA scaffold with surface immobilized collagen and basic fibroblast growth factor. Biomaterials 2005;26:1253–1259. doi:10.1016/j.biomaterials.2004.04.031. [PubMed: 15475055]
56. Lee H, Dellatore SM, Miller WM, Messersmith PB. Mussel-inspired surface chemistry for multifunctional coatings. Science 2007;318: 426–430. doi:10.1126/science.1147241. [PubMed: 17947576]
57. Hong S, Kim KY, Wook HJ, Park SY, Lee KD, Lee DY, Lee H. Attenuation of the in vivo toxicity of biomaterials by polydopamine surface modification. Nanomedicine 2011;6:793–801. doi:10.2217/nnm.11.76. [PubMed: 21793672]
58. Wang Z, Li P, Jiang Y, Jia Z, Tang P, Lu X, Ren F, Wang K, Yuan H. Mussel-inspired nanostructured coatings assembled using polydopamine nanoparticles and hydroxyapatite nanorods for biomedical applications. Biosurf Biotribol 2017;3:1–10. doi:10.1016/j.bsbt.2017.01.001.
59. Liu F, He X, Zhang J, Chen H, Zhang H, Wang Z. Controllable synthesis of polydopamine nanoparticles in microemulsions with pH-activatable properties for cancer detection and treatment. J Mater Chem B 2015;3:6731–6739. doi:10.1039/C5TB01159K.
60. Wang Z, Wang K, Zhang Y, Jiang Y, Lu X, Fang L, Gan D, Lv C, Zhang H, Qu S. Protein-affinitive polydopamine nanoparticles as an efficient surface modification strategy for versatile porous scaffolds enhancing tissue regeneration. Part Part Syst Charact 2016; 33:89–100. doi:10.1002/ppsc.201500187.
61. Takezawa T, Mori Y, Yoshizato K. Cell culture on a thermo-responsive polymer surface. Biotechnology 1990;8:854–856. doi: 10.1038/nbt0990-854. [PubMed: 1366797]

62. Higuchi A, Aoki N, Yamamoto T, Miyazaki T, Fukushima H, Tak TM, Jyujyoji S, Egashira S, Matsuoka Y, Natori SH. Temperature-induced cell detachment on immobilized pluronic surface. J Biomed Mater Res A 2006;79A:380–392. doi:10.1002/jbm.a.30773.
63. McBane JE, Sharifpoor S, Cai K, Labow RS, Santerre JP. Biodegradation and in vivo biocompatibility of a degradable, polar/hydrophobic/ionic polyurethane for tissue engineering applications. Biomaterials 2011;32:6034–6044. doi:10.1016/j.biomaterials.2011.04.048. [PubMed: 21641638]
64. Murphy CM, O'Brien FJ. Understanding the effect of mean pore size on cell activity in collagen-glycosaminoglycan scaffolds. Cell Adhes Migr 2010;4:377–381. doi:10.4161/cam.4.3.11747.
65. Kumari J, Kumar A. Development of polymer based cryogel matrix for transportation and storage of mammalian cells. Sci Rep 2017;7:41551. doi:10.1038/srep41551. [PubMed: 28139669]
66. Laiveniece L, Morozovs A. Impact of water on rheological behavior of polyurethane glues. Rural Sustain Res 2016;35. doi:10.1515/plua-2016-0002.
67. Lee DJ, Lee Y-T, Zou R, Daniel R, Ko C-C. Polydopamine-laced biomimetic material stimulation of bone marrow derived mesenchymal stem cells to promote osteogenic effects. Sci Rep 2017;7: 12984. doi:10.1038/s41598-017-13326-y. [PubMed: 29021583]
68. Hu Y, Dan W, Xiong S, Kang Y, Dhinakar A, Wu J, Gu Z. Development of collagen/polydopamine complexed matrix as mechanically enhanced and highly biocompatible semi-natural tissue engineering scaffold. Acta Biomater 2017;47:135–148. doi:10.1016/j.actbio.2016.10.017. [PubMed: 27744068]
69. Xia XC, Chen XW, Zhang Z, Chen X, Zhao WM, Liao B, Hur B. Effects of porosity and pore size on the compressive properties of closed-cell Mg alloy foam. J Magnes Alloy 2013;1:330–335. doi: 10.1016/j.jma.2013.11.006.
70. Rim NG, Kim SJ, Shin YM, Jun I, Lim DW, Park JH, Shin H. Mussel-inspired surface modification of poly(L-lactide) electrospun fibers for modulation of osteogenic differentiation of human mesenchymal stem cells. Colloids Surf B Biointerf 2012;91:189–197. doi:10.1016/j.colsurfb.2011.10.057.
71. Jiang X, Christopherson GT, Mao H-Q. The effect of nanofibre surface amine density and conjugate structure on the adhesion and proliferation of human haematopoietic progenitor cells. Interf Focus 2011;1:725–733. doi:10.1098/rsfs.2011.0033.
72. Lee JH, Jung HW, Kang I-K, Lee HB. Cell behaviour on polymer surfaces with different functional groups. Biomaterials 1994;15: 705–711. doi:10.1016/0142-9612(94)90169-4. [PubMed: 7948593]
73. Engler AJ, Sen S, Sweeney HL, Discher DE. Matrix elasticity directs stem cell lineage specification. Cell 2006;126:677–689. doi: 10.1016/j.cell.2006.06.044. [PubMed: 16923388]
74. Holle AW, Engler AJ. Cell rheology: Stressed-out stem cells. Nat Mater 2010;9:4–6. doi:10.1038/nmat2589. [PubMed: 20019660]
75. Saha K, Keung AJ, Irwin EF, Li Y, Little L, Schaffer DV, Healy KE. Substrate modulus directs neural stem cell behavior. Biophys J 2008;95:4426–4438. doi:10.1529/biophysj.108.132217. [PubMed: 18658232]
76. Ding YH, Floren M, Tan W. Mussel-inspired polydopamine for bio-surface functionalization. Biosurf Biotribol 2016;2:121–136. doi:10.1016/j.bsbt.2016.11.001. [PubMed: 29888337]
77. Ku SH, Park CB. Human endothelial cell growth on mussel-inspired nanofiber scaffold for vascular tissue engineering. Biomaterials 2010; 31:9431–9437. doi:10.1016/j.biomaterials.2010.08.071. [PubMed: 20880578]
78. Ku SH, Ryu J, Hong SK, Lee H, Park CB. General functionalization route for cell adhesion on non-wetting surfaces. Biomaterials 2010;31:2535–2541. doi:10.1016/j.biomaterials.2009.12.020. [PubMed: 20061015]
79. Yang K, Lee JS, Kim J, Bin Lee Y, Shin H, Um SH, Kim JB, Park KI, Lee H, Cho SW. Polydopamine-mediated surface modification of scaffold materials for human neural stem cell engineering. Biomaterials 2012;33:6952–6964. doi:10.1016/j.biomaterials.2012.06.067. [PubMed: 22809643]
80. Kao C-T, Lin C-C, Chen Y-W, Yeh C-H, Fang H-Y, Shie M-Y. Poly(-dopamine) coating of 3D printed poly(lactic acid) scaffolds for bone tissue engineering. Mater Sci Eng C 2015;56:165–173. doi: 10.1016/j.msec.2015.06.028.

81. Bin Lee Y, Shin YM, hye Lee J, Jun I, Kang JK, Park JC, Shin H. Polydopamine-mediated immobilization of multiple bioactive molecules for the development of functional vascular graft materials. Biomaterials 2012;33:8343–8352. doi:10.1016/j.biomaterials.2012.08.011. [PubMed: 22917738]

82. Lynge ME, van der Westen R, Postma A, Städler B. Polydopamine—A nature-inspired polymer coating for biomedical science. Nanoscale 2011;3:4916. () doi:10.1039/c1nr10969c. [PubMed: 22024699]

83. Zhang W, Wang G, Liu Y, Zhao X, Zou D, Zhu C, Jin Y, Huang Q, Sun J, Liu X, Jiang X, Zreiqat H. The synergistic effect of hierarchical micro/nano-topography and bioactive ions for enhanced osseointegration. Biomaterials 2013;34:3184–3195. doi:10.1016/j.biomaterials.2013.01.008. [PubMed: 23380352]

84. Ferrara N, Kerbel RS. Angiogenesis as a therapeutic target. Nature 2005;438:967–974. doi: 10.1038/nature04483. [PubMed: 16355214]

85. Fiaschi-Taesch N, Stewart AF, Garcia-Ocaña A. Improving islet transplantation by gene delivery of hepatocyte growth factor (HGF) and its downstream target, protein kinase B (PKB)/Akt. Cell Biochem Biophys 2007;48:191–199. doi:10.1007/s12013-007-0024-7. [PubMed: 17709889]

86. Ruvinov E, Leor J, Smadar SC. The effects of controlled HGF delivery from an affinity-binding alginate biomaterial on angiogenesis and blood perfusion in a hindlimb ischemia model. Biomaterials 2010;31: 4573–4582. doi:10.1016/j.biomaterials.2010.02.026. [PubMed: 20206988]

87. Shin YM, Bin Lee Y, Kim SJ, Kang JK, Park JC, Jang W, Shin H. Mussel-inspired immobilization of vascular endothelial growth factor (VEGF) for enhanced endothelialization of vascular grafts. Biomacromolecules 2012;13:2020–2028. doi:10.1021/bm300194b. [PubMed: 22617001]

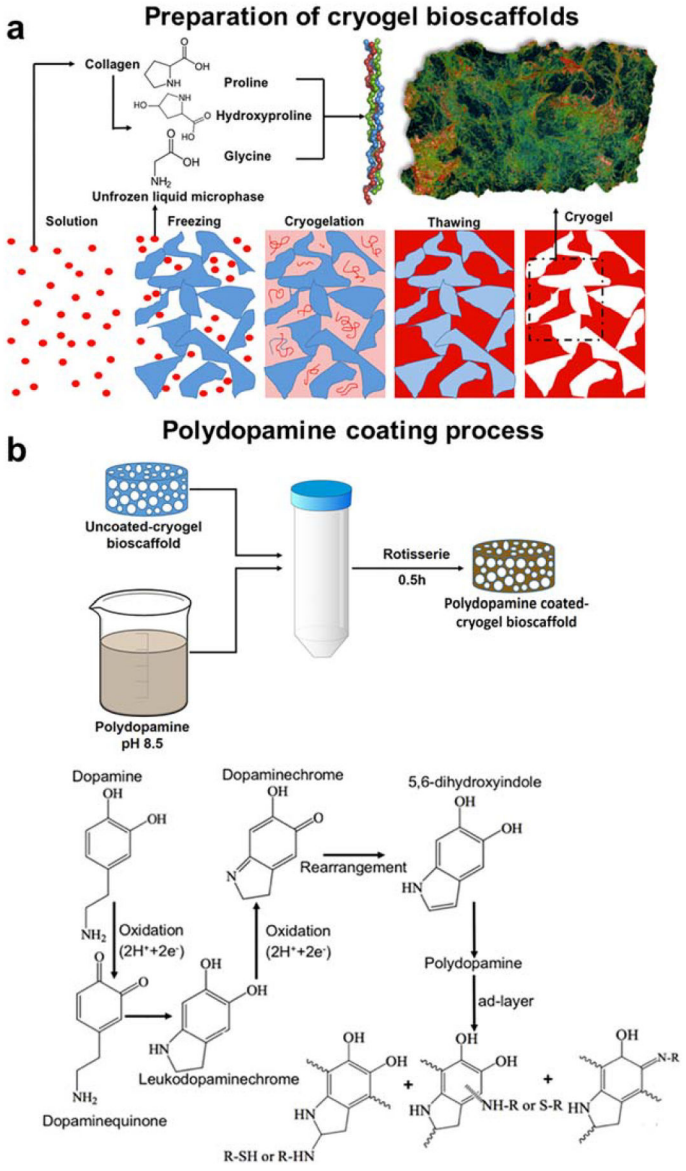

FIGURE 1.

Schematic illustration of the preparation of uncoated- and polydopamine coated-cryogel bioscaffolds: (a) Collagen was swollen overnight in HCl at 4°C and then the collagen dispersion was homogenized and centrifuged. After transferring the collagen slurry to a mold, NHS/EDC was added (depicted as the solution); The molds were kept in a freezer at −20°C for 24 h (depicted as the freezing) to complete the crosslinking process (depicted as the cryogelation). Next, bioscaf-folds were thawed at room temperature (depicted as the thawing); (b) Polydopamine was then coated by immersion of bioscaffolds into a dopamine solution (2 mg/ml in 10 m*M* Tris, pH 8.5) on a tube rotisserie; Schematic illustration of the polydopamine formation mechanism which involves the oxidation of catechol in dopamine to quinone by alkaline pH-induced oxidation.

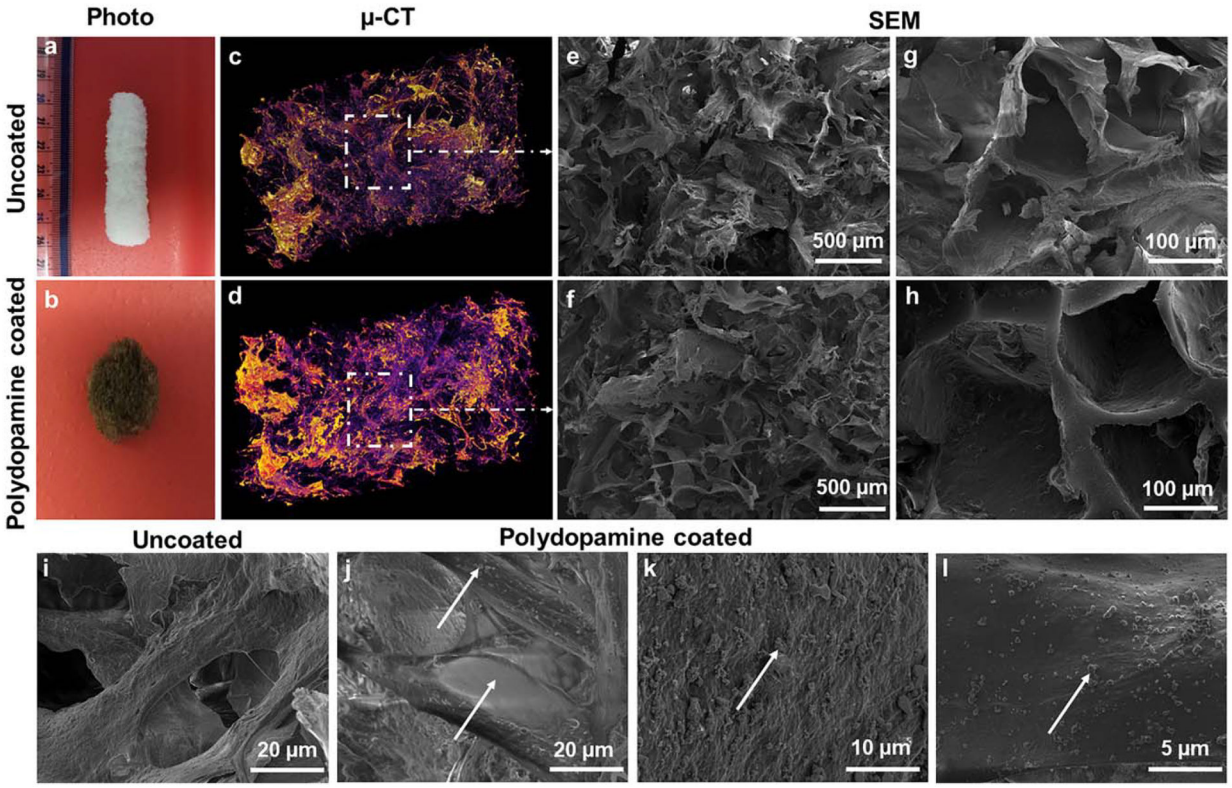

FIGURE 2.

Photographs of an uncoated- (a) and polydopamine coated- (b) cryogel bioscaffold showing the macrostructure and the color change from white to brown with polydopamine coating; The reconstructed μ-CT images of an uncoated- (c) and polydopamine coated- (d) cryogel bio-scaffold whereas the purple areas show the bioscaffold material and the dark areas refer to the void space; SEM images of an uncoated- (e and g) and polydopamine coated- (f and h) cryogel bioscaffold showing the existence of both small, large and continuously interconnected macro-pores throughout the entire bioscaffold construct; High magnification SEM images of an uncoated- (i) and polydopamine coated- (j–l) cryogel bioscaffold showing the morphology of polydopamine coating.

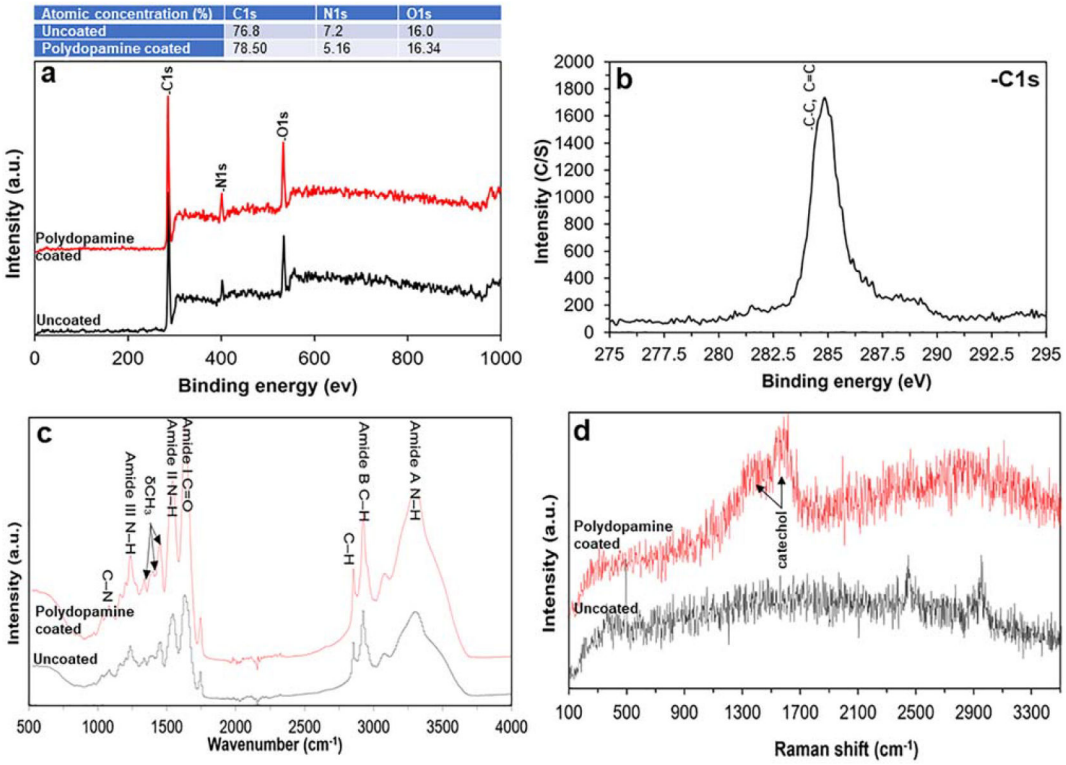

FIGURE 3.

Survey and high-resolution scan XPS spectra showing qualitative XPS spectra of uncoated- and polydopamine coated-cryogel bio-scaffolds along with its quantitative information. (a) The survey spectrum and (b) high-resolution spectra shows three elements of C, O, and N corresponding to the molecular formula which are the basic elements of protein; (c) ATR-FTIR spectrum obtained from uncoated- and polydopamine coated-cryogel bioscaffolds identifying bands corresponding to the amide and three main bands of the collagen fingerprint; (d) The Raman spectra obtained from uncoated- and polydopamine coated-cryogel bioscaffolds demonstrating the characteristic thiol group signal signifying the successful introduction of the thiol group on bioscaffolds surface.

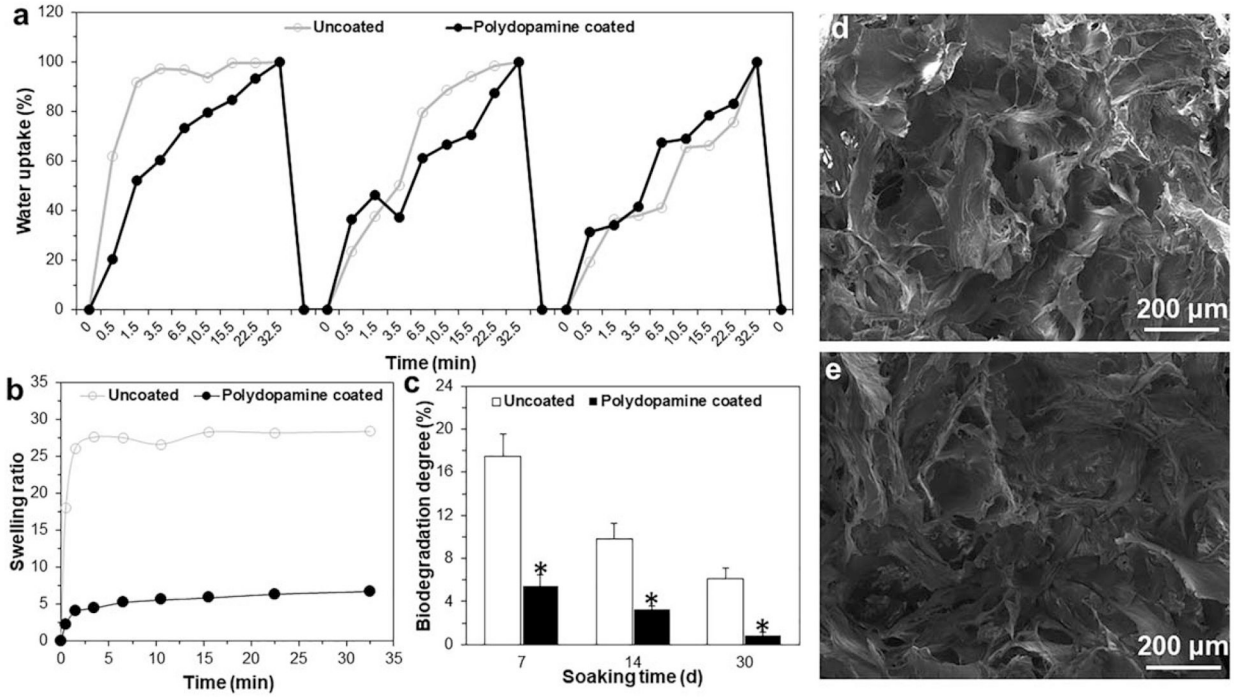

FIGURE 4.

(a) Cyclic water uptake; (b) Swelling kinetics; and (c) Biodegradation degree of bioscaffolds up to four weeks; (d) SEM images of polydopamine coated-cryogel bioscaffold before and (e) after hydration-dehydration process. Significant differences: $*p < 0.05$, difference between uncoated- and polydopamine coated-cryogel bioscaffolds. (Unpaired student's *t* test).

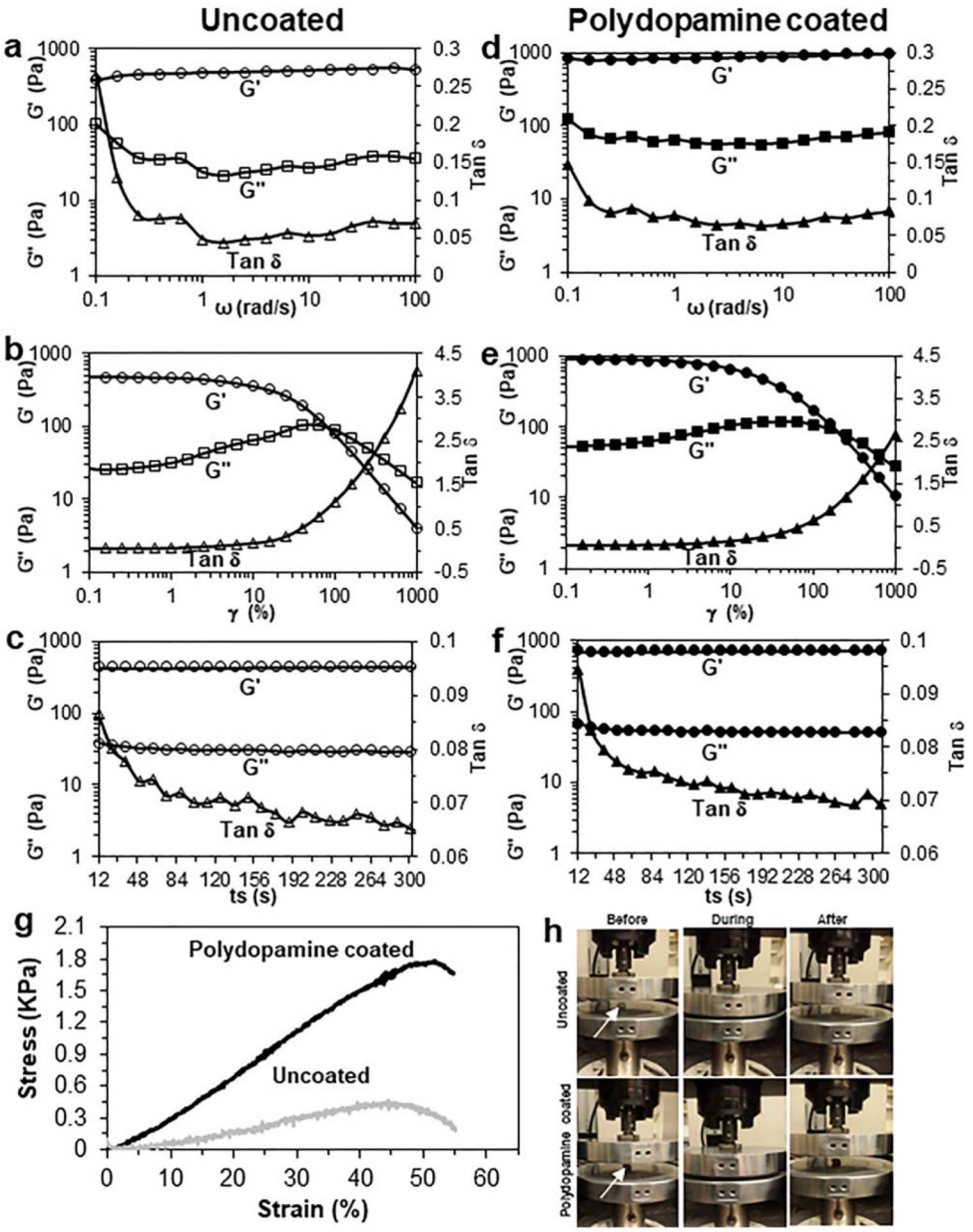

FIGURE 5.

Rheology data of uncoated- (a–c) and polydopamine coated- (d–f) cryogel bioscaffolds: angular frequency (ω) sweep from 0.1 to 100 rad/s (a and d), oscillation strain (γ) sweep from 0.1% to 1000% (b and e) and step time sweep from 0 to 300 s (c and f) of storage modulus (G'), loss modulus (G'') and Tan phase angle (δ) at 37°C in wet state; The compression stress–strain curve of bioscaffolds in wet state (g); The recovery of bioscaffolds to their original shape after removing the load in compression test (h). Significant differences: $p < 0.05$, difference between uncoated- and polydopamine coated-cryogel bioscaffolds. (Unpaired student's *t* test)

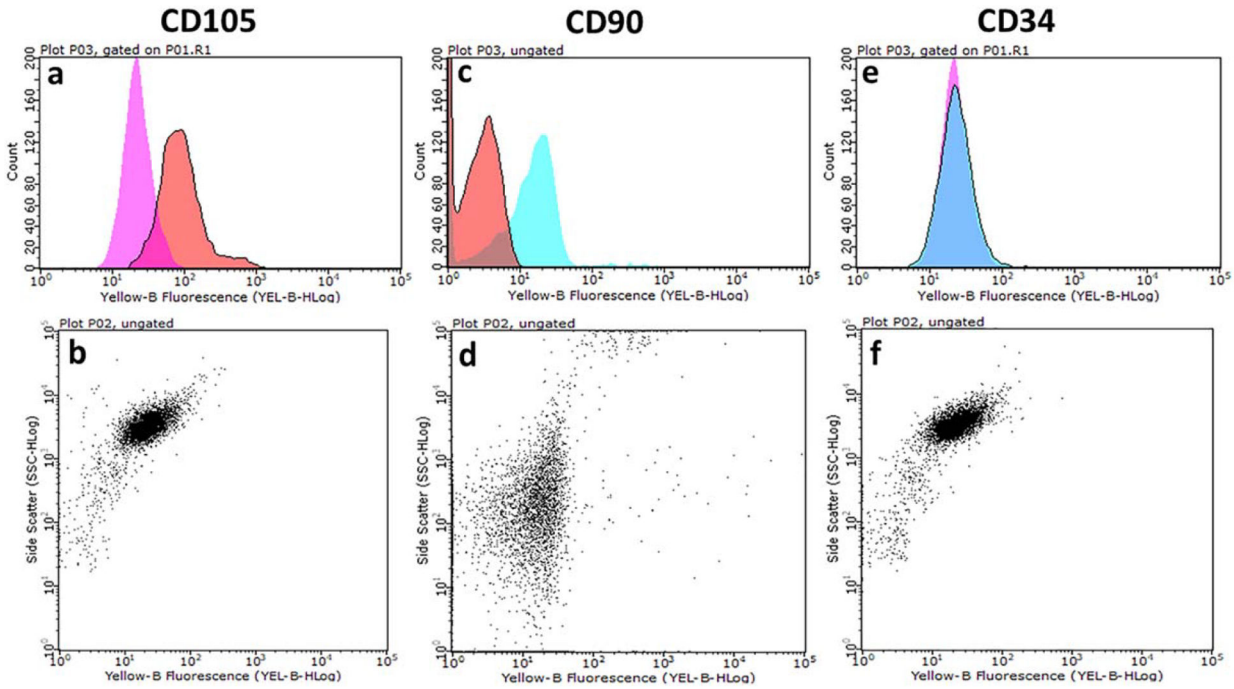

FIGURE 6.

Cell surface expression of various AD-MSCs markers was detected by staining with specific monoclonal antibodies and analyzed by flow cytometry. AD-MSCs are CD105 (a and b) and CD90 (c and d) positive and CD34 (e and f) negative.

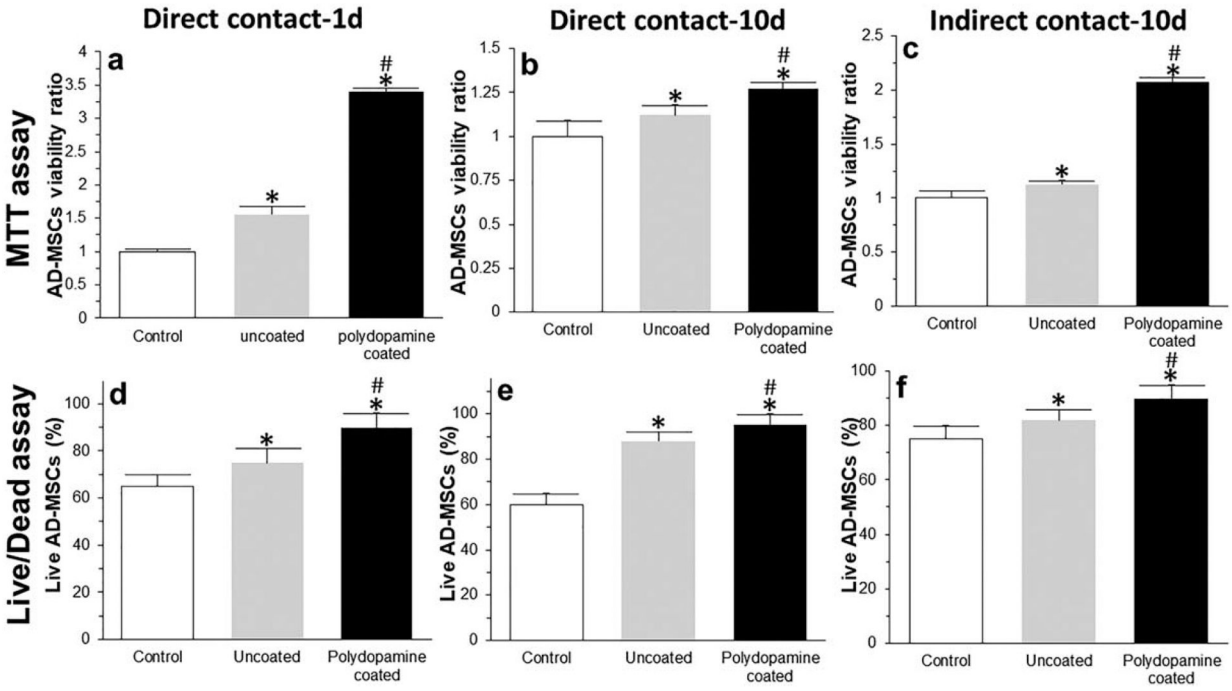

FIGURE 7.

MTT (a–c) and Live/Dead (d–f) assays from both direct (a, b, d, and e) and indirect (c and f) cell culture methods at day 1 (a and d) and 10 (b, c, e, and f). Significant differences: $*p < 0.05$, difference between the control group and bioscaffolds. $^{\#}p < 0.05$, difference between uncoated- and polydopamine coated-cryogel bioscaffolds. (Unpaired student's *t* test).

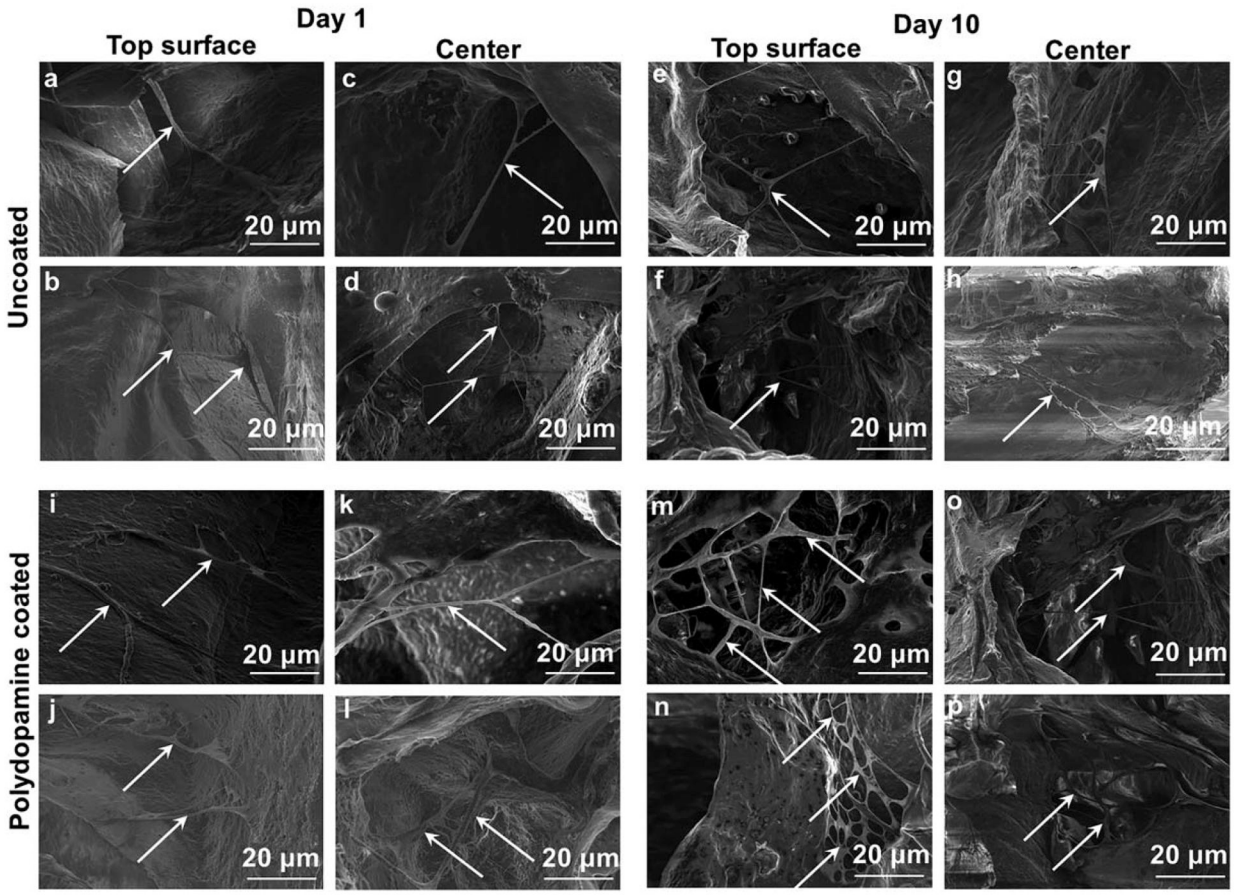

FIGURE 8.

SEM images of AD-MSCs (indicated by white arrows) on the superficial layer (a, b, e, f, i, j, m, and n) and within the center (c, d, g, h, k, l, o, and p) of uncoated- (a–h) and polydopamine coated- (i–p) cryogel bioscaffolds at day 1 (a–d and i–l) and 10 (e–h and m–p).

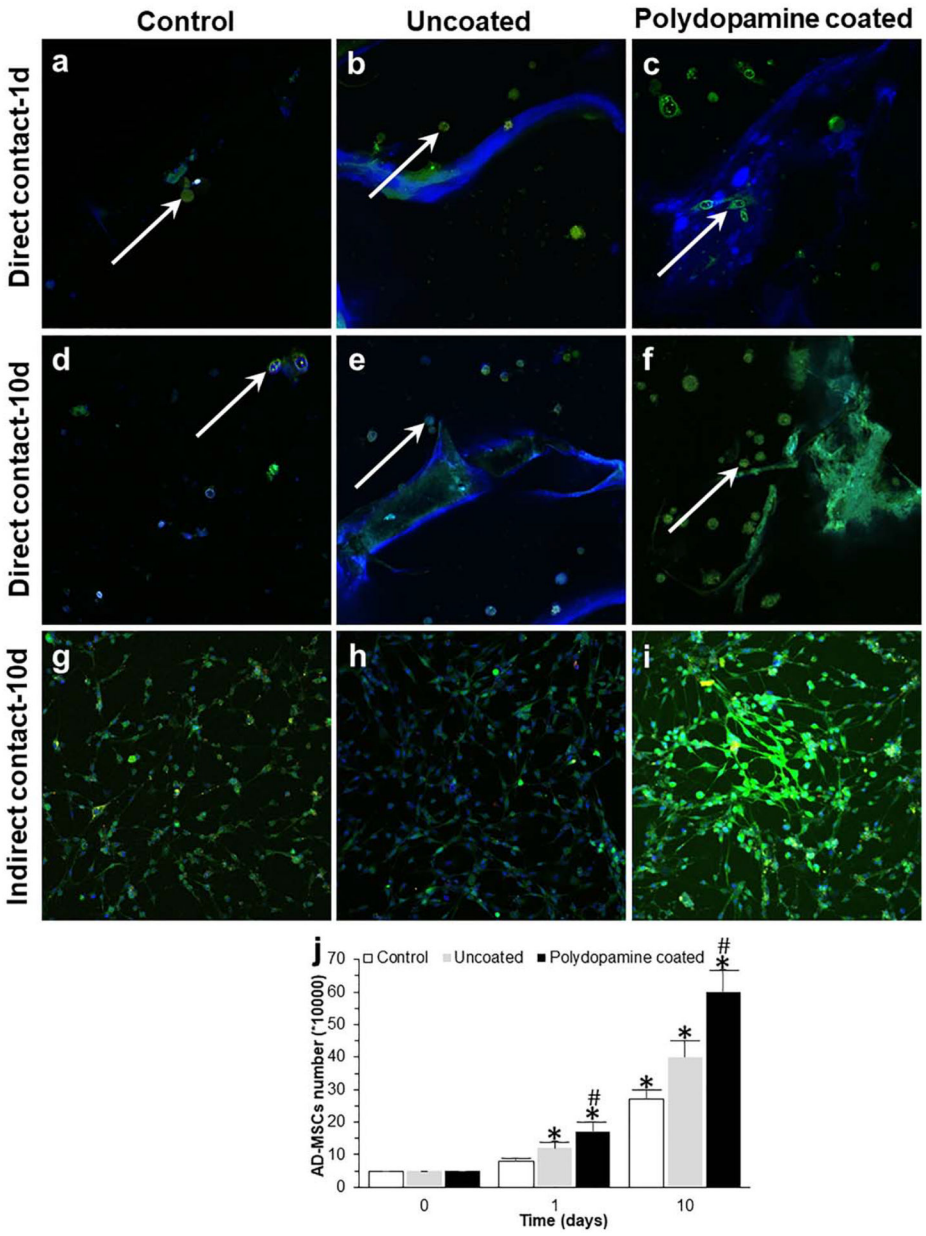

FIGURE 9.

Confocal images of AD-MSCs after 1 (a–c) and 10 (d–i) days seeding into uncoated- (b and e) and polydopamine coated- (c and f) cryogel bioscaffolds (direct contact: a–f) and culturing with the medium of uncoated- (h) and polydopamine coated- (i) cryogel bioscaffolds (indirect contact: g–i) and the results of AD-MSCs counting at day 0, 1, and 10 (j). Significant differences: $*p < 0.05$, difference between the control group and bioscaffolds. $^{\#}p < 0.05$, difference between uncoated- and polydopamine coated-cryogel bioscaffolds. (Unpaired student's *t* test).